NeuroImage 190 (2019) 232–241

Contents lists available at ScienceDirect

NeuroImage

journal homepage: www.elsevier.com/locate/neuroimage

Two cortical deficits underlie amblyopia: A multifocal fMRI analysis

Reza Farivar [a,**,1], Jiawei Zhou [b,*,1], Yufeng Huang [c], Lixia Feng [d], Yifeng Zhou [c], Robert F. Hess [a]

[a] McGill Vision Research, Dept. Ophthalmology, McGill University, The Research Institute of the McGill University Health Centre, Montreal, PQ, Canada
[b] School of Ophthalmology and Optometry and Eye Hospital, State Key Laboratory of Ophthalmology, Optometry and Vision Science, Wenzhou Medical University, Wenzhou, Zhejiang, PR China
[c] CAS Key Laboratory of Brain Function and Disease, School of Life Sciences, University of Science and Technology of China, Hefei, Anhui, 230027, PR China
[d] Department of Ophthalmology, First Affiliated Hospital, Anhui Medical University, Hefei, Anhui, PR China

ARTICLE INFO

Keywords:
Amblyopia
BOLD
Visual acuity
Multifocal
Distortion

ABSTRACT

Amblyopia is a relatively common (incidence 3%) developmental disorder in which there is loss of vision as a consequence of a disruption to normal visual development. Although the deficit is monocular and known to be of cortical origin, the nature of the processing deficit is controversial. Human behavioral studies have identified two main deficits — a loss of contrast sensitivity and perceived spatial distortions. Here we use a multifocal fMRI approach to ascertain, in a group of anisometropic amblyopes, whether these two deficits have a single common cause or whether they are the result of two underlying independent cortical disorders. We found that fMRI magnitudes were attenuated in amblyopic eye stimulation, and that there was poor fidelity for co-localization of the activity clusters between the amblyopic and fellow-fixing eye stimulation. These effects varied across eccentricities and correlate with the degree of amblyopia but not with one another, suggesting two independent cortical deficits: a reduced responsiveness as well as reduced fidelity of spatial representation. These deficits are independent of eccentricity within the central field and consistent across early cortical visual areas.

1. Introduction

Amblyopia, the anomalous monocular visual function due to developmental binocular disruption, is often only characterized by reduced acuity and sensitivity to high spatial frequencies (SF) in the amblyopic eye, despite the prevalence of spatial distortions and suppression. The focus on contrast and high SF loss (Gstalder and Green, 1971; Hess and Howell, 1977; Levi and Harwerth, 1977) has had only partial success in establishing comprehensive animal models of the disorder (Chino et al., 1983; Crewther and Crewther, 1990; Eggers and Blakemore, 1978; Kiorpes et al., 1998) or determining the full extent of the neurophysiological disorder in humans using neuroimaging (Barnes et al., 2001; Li et al., 2007a; Muckli et al., 2006). In studies that reported neurophysiological or neuroimaging anomalies in amblyopia, these have been insufficient in explaining the observed behavioral deficits and correlated poorly with reduced acuity (Barnes et al., 2001; Eggers and Blakemore, 1978; Kiorpes and McKee, 1999; Li et al., 2007a; Movshon et al., 1987). Thus while high SF and contrast perception impairment are important features of the disease, they appear to be insufficient descriptors of the disease.

Amblyopes perceive distinct global spatial distortions (Hess et al., 1978; Lagreze and Sireteanu, 1991; Sireteanu et al., 1993), they mislocalize the position of local features and they are inaccurate in the encoding of spatial position (Bedell and Flom, 1981, 1983; Bedell et al., 1985; Hess and Holliday, 1992; Levi and Klein, 1983; Levi et al., 1985), suggesting an altogether altered representation of visual space that has profound effects for localized judgements when viewing through their amblyopic eye (Bedell and Flom, 1981, 1983; Hess and Holliday, 1992; Levi et al., 1985, 1987; Mansouri et al., 2009)—the full range of symptoms more accurately reflects Tarachopia which means *distorted sight* (Hess, 1982), rather than amblyopia or *blunt sight*.

Spatial distortions, such as those reported between the amblyopic eyes and fellow-fixing eyes, are unlikely to be due to an afferent projection abnormality because such a static deficit would be subject to recalibration during visual development based on the correlation of neural activity. A more likely explanation is one involving anomalous spatial interactions in the cortical retinotopic map (Hess and Field, 1994). Amblyopia induced in young kittens as a result of monocular occlusion or strabismus results in a profound loss in acuity as well as in

** Corresponding author.
* Corresponding author. Wenzhou Medical University, 270 Xueyuan Xi Road, Wenzhou, Zhejiang, 325207, China.
E-mail addresses: reza.farivar@mcgill.ca (R. Farivar), zhoujw@mail.eye.ac.cn (J. Zhou).
[1] Co-first authors.

https://doi.org/10.1016/j.neuroimage.2017.09.045
Received 25 May 2017; Accepted 20 September 2017
Available online 21 September 2017

the spatial representation in the cortex (i.e. distortions in the representation of visual space) which remains after recovery of visual acuity (Gingras et al., 2005a,b). Consistent with this, monkeys with anisometropic amblyopia exhibit a mapping irregularity from V1 to V2 such that the subunits in extra-striate receptive fields are disordered (Tao et al., 2014). A distortion in the retinotopy of cortical area V1 has been reported for the input from the amblyopic eye in human amblyopes as compared to fellow-fixing eye viewing (Li et al., 2007b) and has been shown to be due to dislocation of the position of population receptive fields representing the amblyopic input (Clavagnier et al., 2015). The relationship of this cortical mapping disorder to the reduced visual acuity in amblyopia, which is its key clinical feature, is not known.

Amblyopia in humans and in animal models involves reduced contrast sensitivity/acuity and spatial distortions. It is not clear whether these are two independent deficits that result as a consequence of a disrupted binocular development or whether they are part of a single deficit. To answer this question in humans using neuroimaging one would want to know the relationship between the difference in magnitude and in localization of cortical responses driven by the amblyopic eye with that by the fellow eye. Retinotopic mapping and population receptive field (pRF) estimates utilize predictable stimulation that spans a large patch of cortex. The predictability of the stimuli may bias the responses and mask the neurophysiological response (Esterman and Yantis, 2010; Huk and Heeger, 2000) particularly when investigating local spatial interactions. We therefore sought to evaluate the responsivity (i.e. BOLD amplitude) associated with amblyopia and the response localization fidelity in a surface-based analysis approach with a model-free and unpredictable stimulation paradigm using a multifocal approach analogous to Vanni et al. (2005). We found a pattern of deficits in response magnitude and response localization that correlated well with the clinical manifestation of amblyopia but not with one another.

2. Materials and methods

2.1. Subjects

Twenty adults with anisometropic amblyopia (4 females; average age 24.15 ± 2.21 years old) and 10 control observers with normal or corrected to normal vision (4 females; average age 25.24 ± 1.18 years old) participated in this study. None of the participants had a history of psychiatric or neurological disorder, head trauma or substance abuse. A standard clinical workup was performed on all participants by the 4th author, who is an ophthalmologist. Amblyopes had 2-line or greater inter-ocular difference in the best-corrected visual acuity (≥0.20 logMAR units) and had central fixation (assessed by using the direct-view ophthalmoscope). Clinical details for the twenty amblyopic participants are provided in Table 1. All participants granted informed consent, in accordance with the Wenzhou Medical University, McGill University, Anhui Medical University and University of Sciences and Technology of China Guidelines on Research Ethics.

Table 1
Clinical data for the amblyopes.

Subject	Age/Sex	Eye	Refraction errors	Corrected Visual acuity (logMAR)	Stereo acuity (arc seconds)
A1	26/M	FE	−1.25DS/+0.50DC × 90	0.00	200–400
		AE	+1.00DS/+1.00DC × 90	0.22	
A2	28/M	FE	−1.25DS/	0.10	>800
		AE	+6.50DS/+2.00DC × 10	1.30	
A3	24/F	FE	−2.25DS/	0.00	>800
		AE	+5.00DS/+0.50DC × 75	0.92	
A4	21/M	FE	−3.00DS/	0.10	400
		AE	+2.50DS/	0.60	
A5	24/M	FE	Plano	0.00	>800
		AE	+3.00DS/+2.00DC × 100	0.60	
A6	24/M	FE	−1.25DS/	0.00	>800
		AE	+4.00DS/	0.30	
A7	26/M	FE	−3.00DS/	0.10	200–400
		AE	+2.50DS/+2.50DC × 15	0.40	
A8	23/M	FE	−3.00DS/+1.00DC × 100	0.00	100
		AE	−1.00DS/+3.50DC × 85	0.30	
A9	25/M	FE	−2.25DS/	0.10	>800
		AE	+3.00DS/+1.50DC × 75	0.70	
A10	27/M	FE	+0.50DS/+1.50DC × 180	0.10	800
		AE	+4.00DS/+1.00DC × 170	0.52	
A11	22/M	FE	Plano	0.00	>800
		AE	+2.50DS/+1.50DC × 85	0.40	
A12	25/M	FE	Plano	0.00	100
		AE	+1.00DS/+1.50DC × 95	0.30	
A13	26/F	FE	Plano	0.00	>800
		AE	+2.00DS/+1.00DC × 90	0.70	
A14	22/M	FE	−2.50DS/	0.00	200–400
		AE	+2.00DS/+0.50DC × 96	0.40	
A15	21/M	FE	+0.5DS/+1.00DC × 65	0.00	>800
		AE	+5.5DS/+1.5DC × 90	1.00	
A16	20/F	FE	−1.00DS/+0.50DC × 90	0.10	>800
		AE	+1.50DS/+3.00DC × 100	0.92	
A17	25/M	FE	−3.25DS/	0.10	>800
		AE	+3.50DS/+2.00DC × 80	1.00	
A18	24/M	FE	−0.50DS/	0.00	100
		AE	+2.50DS/+0.50DC × 90	0.40	
A19	27/M	FE	Plano	0.00	>800
		AE	+0.45DS/+0.5DC × 180	0.30	
A20	23/F	FE	−2.75DS/	0.00	200–400
		AE	+1.50DS/	0.40	

Note: FE, Fellow eye; AE, Amblyopic eye; DS, diopter of spherical; DC, diopter of cylinder. Stereo acuity was measured with Titmus.

2.2. Stimuli

The stimulation paradigm used in this study is highly comparable to a multifocal approach previously published by Vanni et al. (2005). The details of our stimulation are provided below, but in brief, the stimulation paradigm involves multiple points of the visual field being stimulated in parallel, with each location being stimulated with a different stimulation schedule. We minimized the correlation between the stimulation schedules for each site so as to improve our ability to detect the activity peaks using conventional General Linear Model (GLM).

All stimuli were generated by a PC running Matlab (MathWorks.Inc.) with PsychToolbox 3.0.9 extensions (Brainard, 1997; Pelli, 1997).

2.2.1. Stimulus generation

Each stimulation "event" at a single visual field location consisted of a 2 × 2 checkerboard pattern, oriented at one of the six designated orientations (0°, 45°, 135°, 180°, 225° and 315°), presented with contrast reversal at 7.5 Hz (Fig. 1a). Each event lasted one second. The checkerboard pattern had its edges blurred by a Gaussian envelope, whose standard deviation was 1/10 of the checkerboard pattern. The checkerboard pattern was initially rendered as a 200 × 200 pixel image, and was then log-polar transformed and scaled to follow the cortical magnification factor for different eccentricities. The size of the checkerboard pattern was 2.7% of the width of the screen for the smallest eccentric (E1), 5.4% for the medium eccentric (E2) and 10.8% for largest eccentric (E3). The checkerboard patterns were essentially symmetric with respect to the screen center at a certain distance (E1: 0.05 × width of the screen; E2: 0.1 × width of the screen; E3: 0.2 × width of the screen). Six designated locations (polar angle at 0°, 45°, 135°, 180°, 225° and 315°; Fig. 1b) were examined in this study. All locations were stimulated in parallel, based on optimal presentation schedules described below. Two positions at the vertical meridian were also shown but not analyzed, because it was not possible to determine the peak location of stimulation for these points as they tended to be split between the two hemispheres.

2.2.2. Optimal presentation patterns for the checkerboard "events"

Temporal correlation between stimulation events occurring at different retinal locations can impede the GLM analysis of the fMRI signal. To minimize this correlation, simulations were carried out with randomly selected event patterns convolved with the canonical hemodynamic response function (HRF). For each simulated time series, 80 events were randomly distributed in time, with a mean of 5 s and standard deviation of 3 s between them, with the additional constraint of minimum 1 s inter-stimulus interval. The event array was then convolved with the hemodynamic response function and the process was repeated to generate 100,000 simulated time series.

We defined the optimal set of stimulation parameters as one that results in the lowest maximum within-set correlation. To find the best event onset combinations, we calculated the correlation matrix for 1,000,000 combinations of the 100,000 simulated sets. We then rank-ordered the sets by their maximum within-set correlation value and selected the set with the lowest maximum within-set correlation. This optimal presentation sequence was then used to determine the onset time for each stimulus at its designated location, as is illustrated for two designated locations in Fig. 1b. All locations were stimulated in parallel, with the stimulation times ("events") occurring according to the optimal schedule that was determined from the simulations described above.

2.2.3. Visual display

Stimuli were back-projected onto a screen, mounted at the head end of the scanner bore, using an Epson-PV150 video projector (1024 pixels × 768 pixels resolution; 60 Hz refresh rate). The distance between the subject and the screen was 45 cm. The size of the screen was 25.2° × 18.9°. The mean luminance of the screen was 50 cd/m^2. The retinal eccentricity and visual angle of the stimuli were respectively 1.9° and 0.5° for E1, 3.8° and 1° for E2 and 7.6° and 2° for E3 (Fig. 1c). Observers viewed the stimuli monocularly, with a tight-fitting eye patch occluding the untested eye, through an angled mirror mounted above their eyes. The tested eye was alternated on each scan for the participants. The orders of the two tested eyes were randomized across observers. Participants, if needed, wore their full refractive correction during scanning.

To aid fixation stability and maintenance of attention, a central fixation target was presented to the tested eye during the scan. The fixation target was a 0.4° dot, whose color was randomly switched between yellow and red. Observers were asked to press a button when the color changed to red. All observers were well-practiced (accuracy above 90%) prior to the scanning sessions to make sure that they familiarized

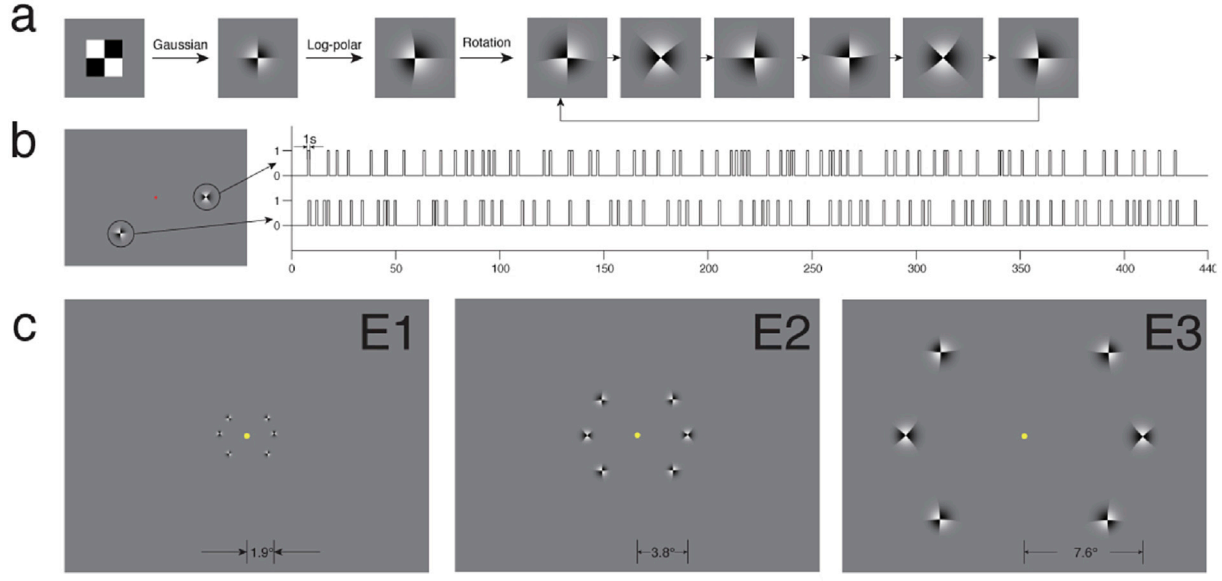

Fig. 1. Visual stimuli and experimental design. a. The checkerboard pattern. Each checkerboard pattern was produced through a Gaussian blur and a log-polar transformation and was presented, with contrast reversing at 7.5 Hz, at one of the 6 designated orientations in different trials; b. In each scan, a multifocal stimulation paradigm was used, whereby each location was stimulated 80 times in parallel-occurring events. The stimulation schedules for each location were chosen from simulations to yield minimal correlation amongst all locations. The onset time at two designated locations are shown here to illustrate the low within-set correlation between stimulation schedules for each location. c. The 6 designated locations investigated in the current study (0°, 45°, 135°, 180°, 225° and 315°). The retinal eccentricity and visual angle were 1.9° and 0.5° for E1, 3.8° and 1° for E2 and 7.6° and 2° for E3.

themselves with the fixation task.

2.3. Magnetic resonance imaging

Scanning was performed at the Anhui Medical University using a GE Signa HDx 3.0 T whole-body with an eight-channel receive-only head coil. Each scanning sessions began with the acquisition of high-resolution three-dimensional T1 weighted images, which were acquired using an IR-FSPGR sequence (TR = 2300 ms; TE = 2.94 ms; flip angle = 9°; 176 slices; voxel size = 1 × 1 × 1 mm^3). Functional scans were then conducted immediately thereafter. Each functional scan consisted of 148 T2*-weighted gradient-echo planar images depicting blood oxygen level-dependent (TR = 2000 ms; TE = 28 ms; flip angle = 72°; 26 slices; voxel size = 1.5 × 1.5 × 2.2 mm^3).

2.4. Processing of MRI images

2.4.1. Anatomical images

The global high-resolution 3-D T1 weighted anatomic images were analyzed by using Freesurfer v5.3.0 (http://surfer.nmr.mgh.harvard.edu). Then the MRI data were classified into white and grey matter and turned into the sphere and flattened data (Dale et al., 1999; Fischl et al., 1999; Reuter et al., 2012).

2.4.2. Functional image

Functional images were analyzed using the Analysis of Functional Neuroimages (AFNI) software package (Cox, 1996). To avoid start-up magnetization transients, data that were collected in the first 10 s (five TRs) were removed from each functional run. The fMRI data were slice-time corrected, motion corrected, and temporaly detrended with respect to the head motion and up to order 3 polynomial drift correction and where spatially smoothed with a Gaussian kernel with full width at half maximum (FWHM) of 4 mm. The mean of the corrected image prior to detrending registered to the anatomical image and the calculated transform was used to align the detrended and smoothed data to the anatomical data for surface-based analysis. Data with a head movement larger than 2 mm was removed from further analysis. Standard GLM analysis was performed in 3dDeconvolve using a two-gamma HRF model convolved with the onset of the stimuli and fitted to the fMRI time-series.

2.4.3. Surface based analysis

Functional surface-based analysis was carried out using SUMA (Saad and Reynolds, 2012). Surface data from Freesurfer was first converted to a SUMA format, and the GLM images from AFNI were then projected onto the SUMA-converted cortical surface model for further analysis.

2.4.4. Inter-ocular deviation

The inter-ocular deviation was defined as the Euclidian distance between the peak positions of each stimulus as produced by the stimulation of each eye. For each stimulus position, the voxel position of the activity peak was denoted for the dominant eye, and the peak of the activity cluster within a 3-voxel radius neighborhood in the non-dominant eye was defined as the corresponding peak location in response to stimulation of the non-dominant eye.

2.4.5. Identification of visual areas

Visual field sign (VFS) map was calculated by automatic volumetric segmentation (Warnking et al., 2002) in Freesurfer. Eccentricity and polar-angle phase maps combined with response were analyzed by fast Fourier transformation. Different visual areas could be identified based on an estimate of opposite field signs (Smith et al., 2001).

2.5. Statistical analysis

Repeated-measures analysis of variance (ANOVA) was used to determine the effect of within-subject factors (e.g., eccentricity, visual area, eye) and the between-subject factor (i.e., group) on the spatial deviation scores or the %BOLD amplitude. Independent samples t-tests were carried out to judge if the average deviation scores or the average Bold signal across the six designated locations were significantly different between the two groups at different eccentricities and visual areas. Paired sample t-tests were carried out to judge if there were any differences between the eyes. The correlation between the average inter-ocular deviation or the averaged %BOLD amplitude and the severity of amblyopia were calculated as the Pearson correlation coefficient (ranging between −1 and 1; 2-tailed) and empirical *P* Values from permutation tests (based on 10,000 permutations of the data) were provided to determine if the correlations were significant.

3. Results

3.1. Average %BOLD signal change

Fig. 2 depicts the average %BOLD amplitude across the six designated locations for normals (dominant eye and non dominant eye) and amblyopes (fellow-fixing eye and amblyopic eye) at different eccentricities and visual areas. One subject (A17) was excluded because of an undiscernible response amplitude in areas V3 and E1 in our inter-ocular deviation measure; we therefore confined our statistical analyses to the data from the remaining 19 patients whose V3E1 response was robust. Repeated-measures ANOVA showed that the %BOLD signal change was significantly different between eyes in amblyopes ($F(1, 18) = 9.763$, $p = 0.006$), but not in the normal controls ($F(1, 9) = 0.572$, $p = 0.469$). The results of the fellow eyes of amblyopes were not significantly different from that of the dominant eyes ($F(1, 27) = 0.012$, $p = 0.914$) or non-dominant eyes of controls ($F(1, 27) = 0.004$, $p = 0.951$).

Further repeated-measures within-subject two-way ANOVA for amplyopes revealed that the average inter-ocular ratio of the %BOLD signal change (across the six stimulation positions) was not significantly different between eccentricities ($F(2, 36) = 2.661$, $p = 0.084$) and visual areas ($F(2, 36) = 2.382$, $p = 0.107$). The interaction of these two factors was also not significant ($F(4, 72) = 0.934$, $p = 0.449$).

Fig. 3 illustrates the relationship in amblyopes between the average inter-ocular ratio of the %BOLD signal change across different designated stimulus locations and the inter-ocular logMAR visual acuity difference. Positive correlation was found for all the conditions that we investigated, which was in all cases significant, except at V1E1 and V1E3. To test for the overall relationship between the inter-ocular ratio of %BOLD signal change and inter-ocular logMAR acuity difference, we pooled the Fisher Z-transformed correlation coefficients from the three eccentricities and visual areas and found that the relationship was highly significant overall ($t(8) = 8.263$, $p < 0.00002$).

3.2. Inter-ocular deviation of response location

The average inter-ocular deviation scores at different stimulation positions, eccentricities and visual areas are plotted in Fig. 4 for normals (green) and for amblyopes (red). In general, amblyopes (A) tended to have larger inter-ocular deviation scores than the normal controls (N).

To simplify further statistical analysis, we averaged the results across the six stimulation positions at each eccentricity. We ran a repeated-measures ANOVA, with eccentricity (E1, E2 and E3; 3 levels) and visual area (V1, V2 and V3; 3 levels) as within-subject factors and group (amblyopia and normal control; 2 levels) as between-subject factor for all participants. The analysis showed that the average deviation scores (across the six stimulation positions) were significantly different between groups ($F(1, 27) = 8.622$, $p = 0.007$) and visual areas ($F(2, 54) = 6.196$, $p = 0.004$) and marginally significant between eccentricities ($F(2, 54) = 3.021$, $p = 0.057$), while the interaction among those factors were not significant ($p > 0.06$, for all). Further repeated-measures within-subject two-way ANOVA for each group revealed that the inter-ocular deviation scores were significantly different between visual areas

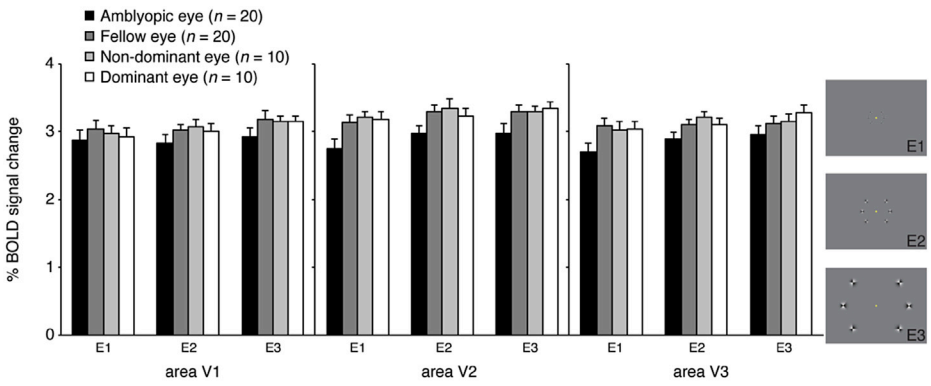

Fig. 2. Average %BOLD signal change. Average %BOLD signal change across the six designated locations at different eccentricities and visual areas for the two groups. Error bars represent standard errors.

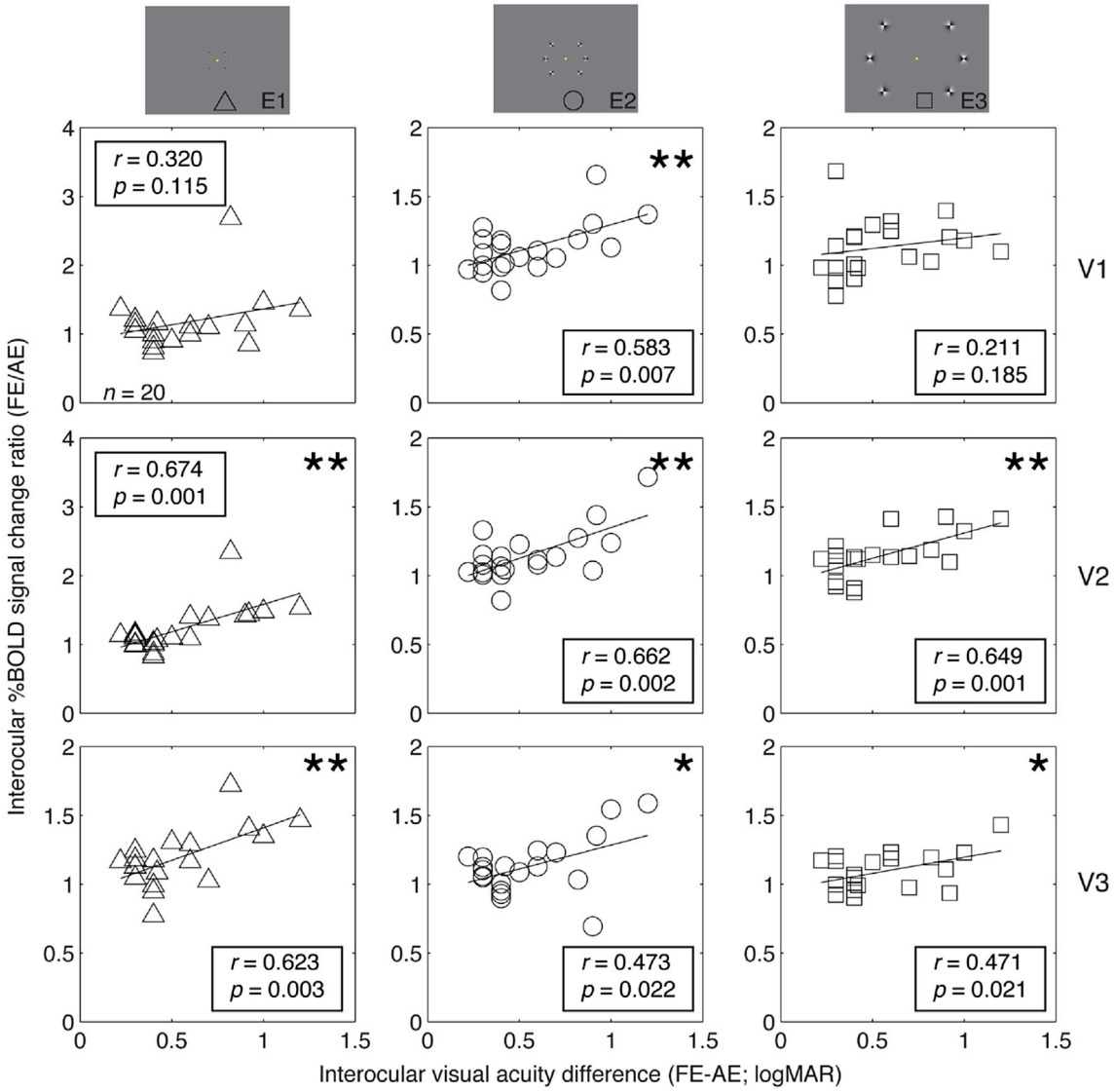

Fig. 3. Relationship between the mean inter-ocular ratio of the %BOLD signal change and the severity of amblyopia. Solid lines represent the best linear fittings. Pearson correlation coefficients and empirical *p* Values from Monte Carlo Procedures (based on 10000-time simulation) are provided for each fitting inside of each panel. *, $p < 0.05$; **, $p < 0.01$.

(amblyopes: $F(2, 36) = 5.617$, $p = 0.008$; normals: $F(2, 18) = 4.624$, $p = 0.024$), but not between eccentricities (amblyopes: $F(2, 36) = 2.843$, $p = 0.071$; normal: $F(2, 18) = 1.824$, $p = 0.19$). The interaction of these two factors was also not significant for either group (amblyopes: $F(4, 72) = 0.777$, $p = 0.544$; normals: $F(4, 36) = 0.389$, $p = 0.815$).

Fig. 5 shows the group difference in the inter-ocular deviation score for normals and amblyopes. Larger inter-ocular deviation was found in amblyopes for all the eccentricities we investigated.

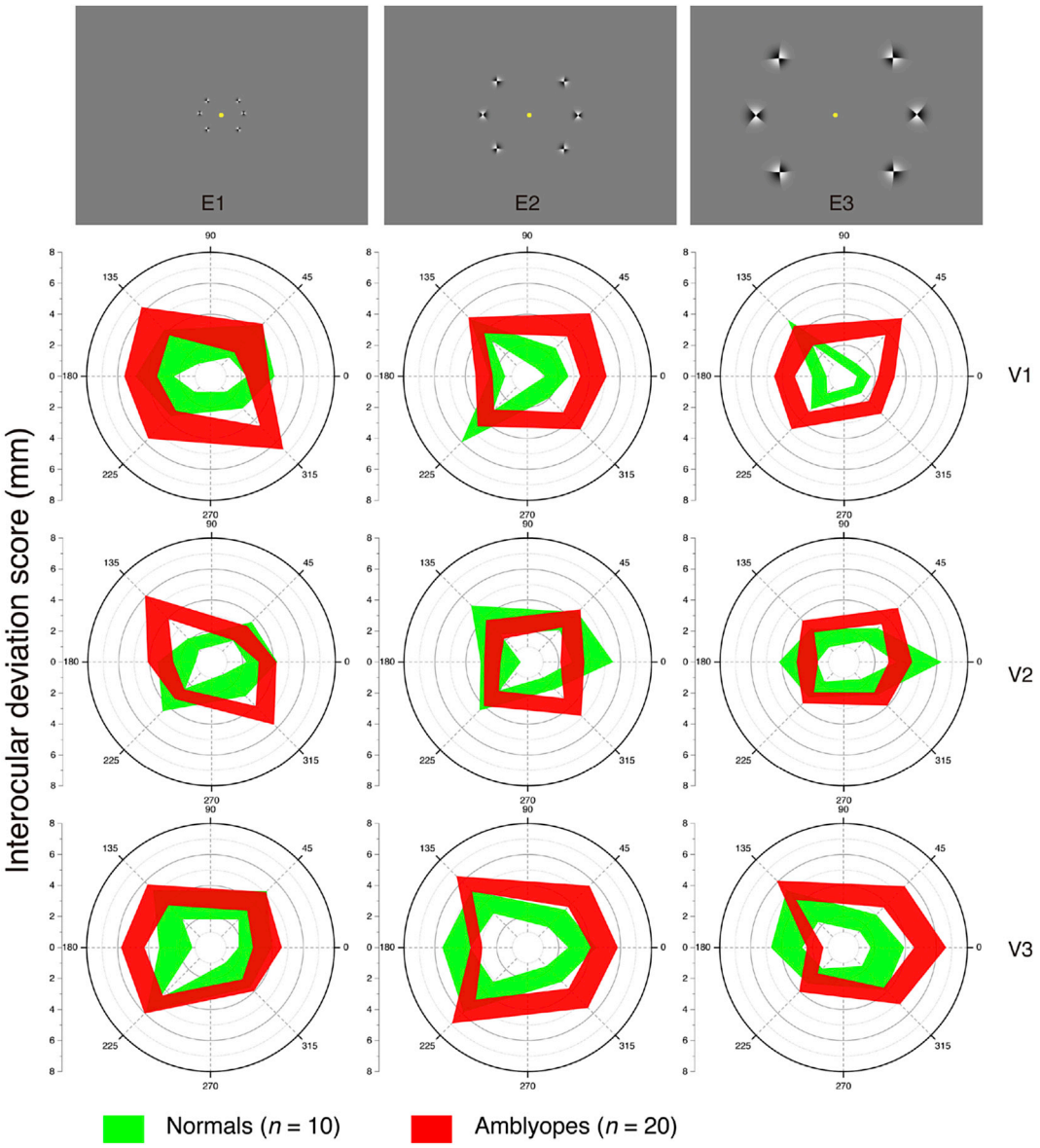

Fig. 4. Inter-ocular deviation scores across positions, eccentricities and visual areas for normals and amblyopes. Average deviation scores were plotted for different eccentricities (in different columns) and visual areas (in different rows) for amblyopes (red) and normal controls (green). The angles (0°, 45°, 135°, 180°, 225° and 315°) of polar diagram represented the six stimulation positions. The width of the band represented the range between 'mean + SE' and 'mean − SE' at each stimulation position.

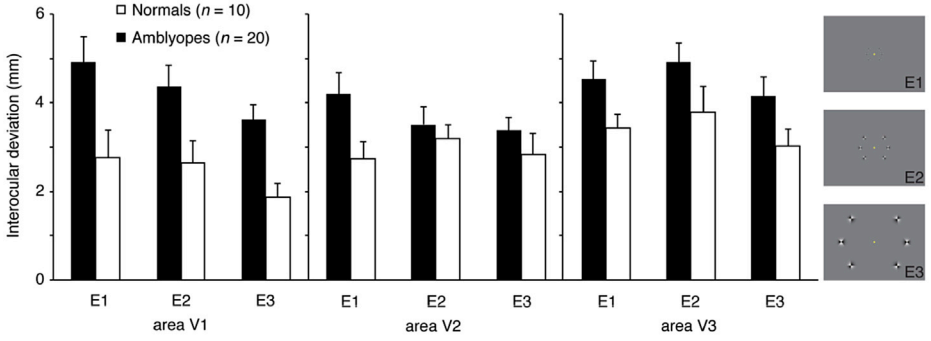

Fig. 5. Average inter-ocular deviation. Average inter-ocular deviation at different eccentricities and visual areas for the two groups. Error bars represent standard error.

Fig. 6 shows the correlation between the inter-ocular deviation of the peak activity location and the severity of amblyopia (i.e., the inter-ocular logMAR visual acuity difference) in different visual areas and eccentricities. Pearson correlation analysis showed that there was a positive correlation between the deviation scores and the severity of amblyopia, which was more evident in E1 and E2 at V1 and V2. To test for the overall relationship between the inter-ocular ratio of peak location deviation and inter-ocular logMAR visual acuity difference, we pooled the Fisher Z-

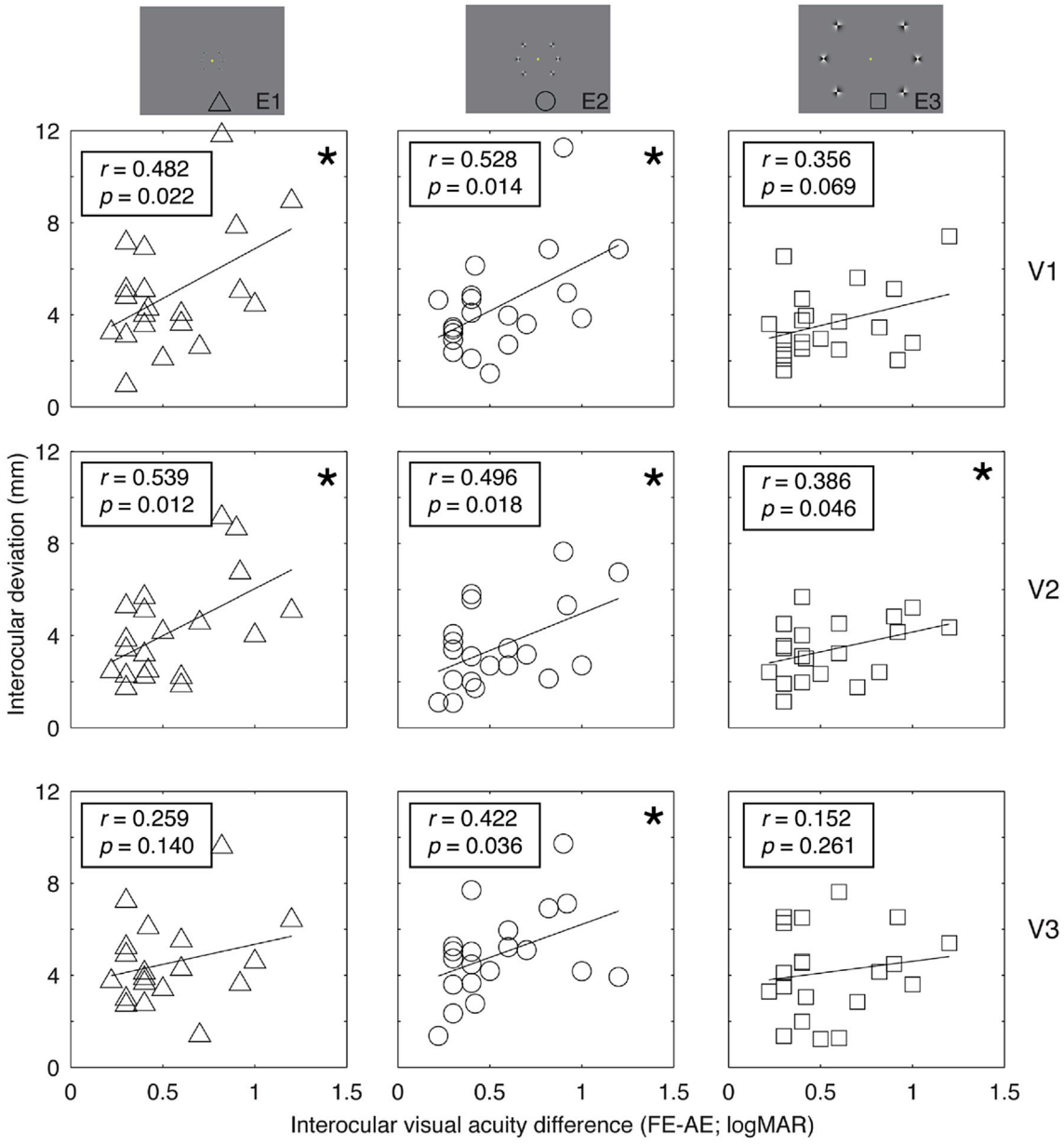

Fig. 6. Relationship between inter-ocular deviation and the severity of amblyopia. Solid lines represent the best linear fittings. Pearson correlation coefficients and empirical *p* Values from permutation tests (based on 10,000 permutations of the data) are provided for each fitting inside of the figure. *, $p < 0.05$.

transformed correlation coefficients from the three eccentricities and visual areas and found that the relationship was highly significant overall ($t(8) = 8.57$, $p = 0.000013$).

As we show above, both the inter-ocular differences in %BOLD signal change and the inter-ocular deviations correlate with the severity of amblyopia. One remaining question is whether there was any correlation between these two brain processing anomalies? To answer this, we plotted the residual of the correlation between the average inter-ocular ratio of the %BOLD signal change and the severity of amblyopia (i.e., results in Fig. 3) and the residual of the correlation between the inter-ocular deviation and the severity of amblyopia (i.e., results in Fig. 6) in Fig. 7. For conditions where there is a strong and significant correlation between both the inter-ocular ratio of %BOLD signal change/inter-ocular deviation and the severity of amblyopia (logMAR visual acuity difference), namely (V1E2, V2E1, V2E2, V2E3 and V3E2), significant correlation between the residual of the two fMRI measures (%BOLD and Deviation) was found only at V3E2 ($p = 0.001$), but not at any other visual areas or eccentricities. To test for the overall relationship between the residual inter-ocular ratio of peak location deviation and the residual %BOLD signal change, we pooled the Fisher Z-transformed correlation coefficients from the three eccentricities and visual areas but failed to find a significant relationship ($t(8) = 1.14$, $p = 0.14$).

4. Discussion

Using small, localized and unpredictable stimulation, we demonstrate two processing anomalies in patients with anisometropic amblyopia — a reduced %BOLD response and an increased scatter or deviation in the response locus within V1, V2 and V3 of the amblyopic eye's cortical representation compared with the fellow eye's cortical representation. Many previous studies have also reported reduced %BOLD response in striate as well as extrastriate (Barnes et al., 2001; Hess et al., 2010b; Lerner et al., 2006; Lerner et al., 2003; Li et al., 2007a) brain regions. Previous studies have used more spatially extended stimuli and have not observed any significant relationship between the %BOLD reduction and the severity of the acuity deficit in amblyopia (Li et al., 2007a). We have

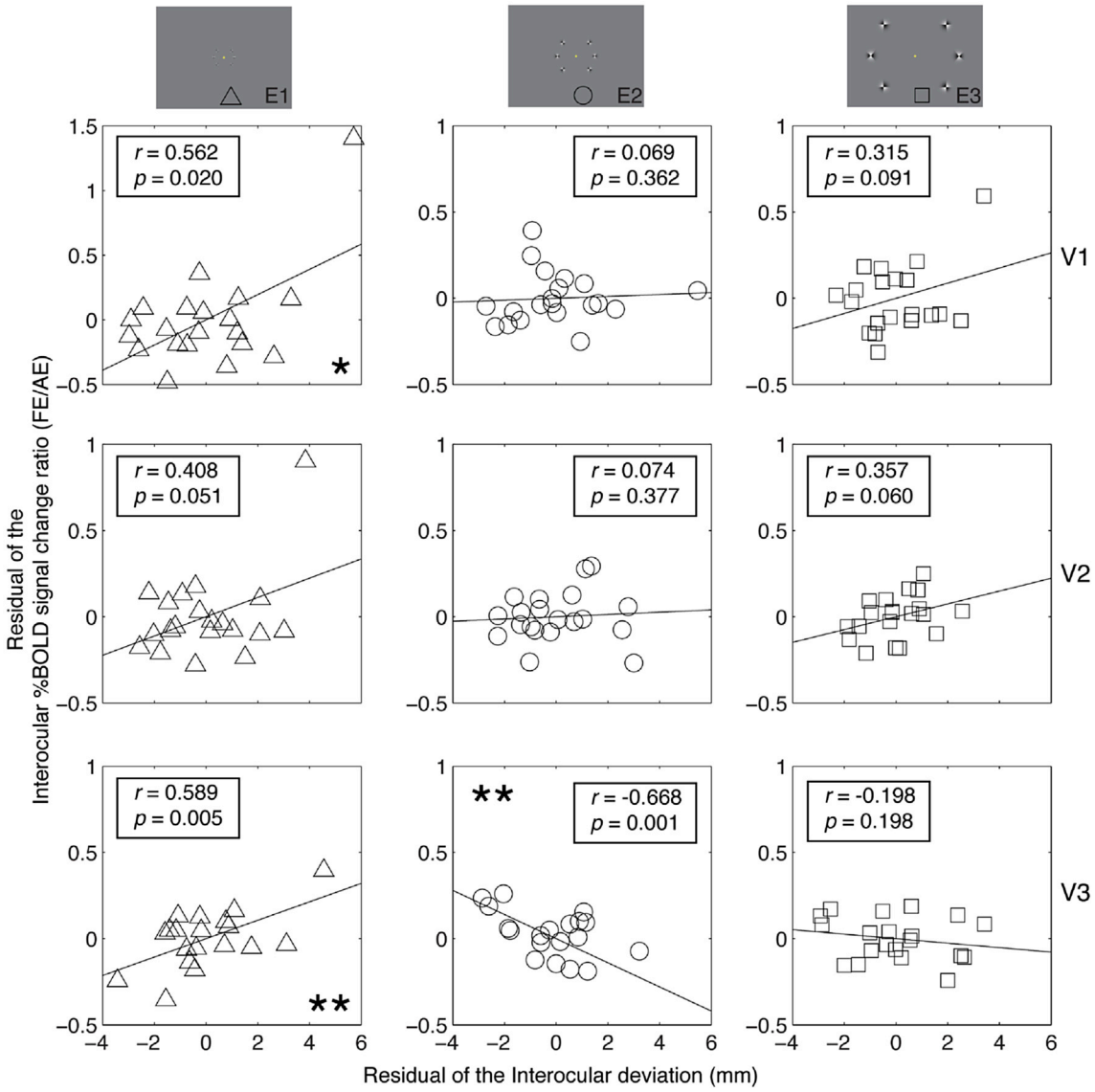

Fig. 7. Relationship between the residual of the inter-ocular ratio of the mean %BOLD signal change and the residual of the inter-ocular deviation. Solid lines represent the best linear fittings. Pearson correlation coefficients and empirical P Values from permutation tests (based on 10,000 permutations of the data) are provided for each fitting inside of the figure. *, $p < 0.05$; **, $p < 0.01$.

revealed such a relationship: the more severe the acuity loss, the more the %BOLD is reduced for most of the eccentricities tested within the central field and across all three visual areas where we conducted our analysis. The %BOLD deficit did not significantly vary as a function of retinal eccentricity or visual area.

We find significantly increased inter-ocular deviation in the peak position of activations for our multifocal stimuli for amblyopes, suggesting a more disordered representation in the amblyopic brain. This deficit is larger in extrastriate areas, but not between different eccentricities. In most visual areas it bears a strong relationship to the severity of amblyopia: the more severe the acuity deficit in amblyopia, the greater the positional disarray. Two previous studies have reported a comparable mapping deficit in amblyopia using different protocols. Li et al. (2007b) using a phase-encoded mapping protocol first demonstrated a more noisy retinotopy in V1 for the amblyopic eye stimulation and Clavagnier et al. (2015), using a population receptive field protocol demonstrated an abnormal scatter in population receptive field position that increased from striate to extrastriate cortex. While both the deficits for magnitude (%BOLD) and location (deviation) positively correlate with the acuity deficit in amblyopia across several eccentricities and visual areas, they are themselves not always correlated, suggesting they may make independent contributions to the amblyopic deficit. Amblyopia is known as a developmental issue (Ciuffreda et al., 1991). Therapies, for example, patching the fellow eye or training the amblyopic eye using visual perceptual learning, have been used to recover the sensitivity loss of the amblyopic eye by using the brain's visual plasticity (for review, see (Levi and Li, 2009) and (Hess et al., 2014)). The mapping (deviation) deficit that we show here suggests that this developmental issue also involves distortions of the cortical retinotopic map, which may be an important consideration in future, therapies.

Our approach and results for studying distortions in cortical visual representations in amblyopia have important and valuable lessons for measuring and understanding the normal human brain. First, our approach confirms the possibility of rapid, unpredictable stimulation as a tool to probe the retinotopic representations of early visual areas (Vanni et al., 2005) and extends this to comparing the *relative* distortions in this map that are presented between amblyopic vs. fellow-fixing viewing. This approach can be used to evaluate other aspects of retinotopic distortions or changes that may accompany alterations to normal visual experience.

Second, our results highlight how cortical response magnitude and spatial position may be related to different aspects of development. Intuitively, a representation with high correspondence to the inputs would represent the same features of the stimulus similarly and in a manner invariant to moderate change. In the case of monocular visual representation, one would expect that the response magnitude and cortical location of representation to be features that are conjoined in a robust visual representation. Our results suggest that response magnitude and spatial representation of those responses may both rely on normal inputs during development, but that they are different and possibly dissociable features of a cortical representation.

4.1. Relationship to animal models and psychophysics

Animal models of amblyopia have revealed single-cell spatial tuning deficits within the central field representation in the striate cortex (Chino et al., 1983; Crewther and Crewther, 1990; Eggers and Blakemore, 1978; Kiorpes et al., 1998; Kiorpes and McKee, 1999; Movshon et al., 1987). These anomalies would be expected to affect contrast coding particularly at higher spatial frequencies and could provide a basis for the known deficits in contrast sensitivity (Hess and Howell, 1977; Kiorpes et al., 1987; Levi and Harwerth, 1977) as well as for the reduced %BOLD responses that we and others (Barnes et al., 2001; Hess et al., 2010a, 2010b; Li et al., 2007a; Sireteanu et al., 1998) have reported using brain imaging. While %BOLD deficits are found in extrastriate areas (Barnes et al., 2001), these could in principle be explain by the striate deficit. It is also accepted that the deficit in amblyopia must extend beyond V1 (Barnes et al., 2001; Kiorpes et al., 1998; Kiorpes and McKee, 1999) and also involve more than just contrast coding (Gingras et al., 2005a; Hess and Field, 1994; Tao et al., 2014) because, behaviorally, there are a host of visual sensitivities affected in addition to contrast (Aaen-Stockdale et al., 2007; Bedell and Flom, 1981; Levi and Klein, 1982; Mansouri et al., 2005; Sharma et al., 2000; Simmers et al., 2003). Prime amongst these is a deficit involving global spatial distortions (Hess et al., 1978; Sireteanu et al., 1993) and anomalous coding of local position (Bedell and Flom, 1981; Levi et al., 1985). This has now been demonstrated using a host of different approaches (Bedell and Flom, 1983; Bedell et al., 1985; Hess et al., 1978; Hess and Holliday, 1992; Levi and Klein, 1983; Levi et al., 1985; Mansouri et al., 2009; Sireteanu et al., 1993) and shown to be separate from the contrast coding abnormality (Hess and Field, 1994; Hess and Holliday, 1992) prompting a redefinition of the condition in terms of Tarachopia (distorted sight) rather than Amblyopia (blunt sight) (Hess, 1982). Recent animal models have identified anomalous mapping of the projections of V1 cells to the subunits of larger V2 cells (Tao et al., 2014). A recent pRF fMRI study in human amblyopes (Clavagnier et al., 2015) has shown that this mapping deficit in V2 cannot be explained by the deficit in V1 and the mapping deficit in V3 cannot be explained by the deficit in V2—there is additional disarray in V2 and in V3. We verify, using a multifocal approach, that such a deficit is present, with different magnitude of inter-ocular deviation in striate and extrastriate areas. Furthermore, we find that the deficits for magnitude (%BOLD) and location (deviation) are not always correlated across our patient groups, suggesting that they may represent different types of brain dysfunction in amblyopia that affect both striate and extrastriate cortex.

4.2. Relationship between the retinotopic distortions in brain imaging and the psychophysically-measured visual field distortions in amblyopia

Only a few studies have tried to quantify the retinotopic nature of the anomaly using punctate stimuli similar to those used here to measure BOLD responses (Hussain et al., 2015). These psychophysical studies document increased localization anomalies of the order of a degree that occur for both central and paracentral regions (7° eccentricity). This cannot be explained by fixation or eye movement instability (Hussain et al., 2015). The most challenging problem in relating these psychophysical anomalies to the fMRI anomalies measured here is that the brain deficit for localization is different in different visual areas (also see (Clavagnier et al., 2015)). Thus, while it is tempting to think of it as a static visual field distortion, it is obviously much more complex and most likely the consequence of inter-ocular, active top-down as well as lateral interactions.

The relationship between perceptual distortions and the neural representation may not be straightforward as there are an indeterminate number of ways that a perceptual distortion could be linked to a disrupted neural representation. We believe perceptual distortions have developed because of an anomalous interaction between the eyes rather than an anomaly, which arises solely in the organization of signals from the amblyopic eye. This is why we have defined the anomaly relative to that of the fellow eye's representation.

4.3. Role of eye movements

There are a number of reasons why we do not think the increased inter-ocular deviation in the position of localized activations corresponding to our multifocal stimuli are due to abnormal eye movements. First, we study exclusively anisometropic amblyopes who all have central fixation (see Methods) and whose fixation eye movements are only mildly abnormal (Chung et al., 2015; Ciuffreda et al., 1979; Niechwiej-Szwedo et al., 2010). Second, larger than normal fixation eye movements would not be expected to, on average, produce displacements in peak location; rather, if there was an effect at all, it would be to reduce peak activation (blurring the activity profile) and result in a larger area of reduced activation and hence a more variable estimation of the location of the peak activity. The %BOLD deficit was not correlated across subjects with deviation deficit. Third, Clavagnier et al. (2015) conclusively show that the population receptive field scatter that they report was not contaminated by eye movements even for strabismic amblyopes who have a much greater eye movement abnormality than the anisometropes used here (their Fig. 6). Finally, any eye movement contribution to the estimation of the location of peak activation would be expected to be invariant with visual area, yet the disarray we report varies significantly with visual area. A similar conclusion has been reached from the psychophysical studies of spatial distortion in amblyopia using punctate stimuli similar to those used here (Hussain et al., 2015; Mansouri et al., 2009).

The distortions that we document vary with the cortical visual area (see also Clavagnier et al., 2015) and therefore are not amenable to an explanation in terms of anomalous eye position. Nor can they be understood in terms of eye position instability as that would have blurred our cortical representation rather than distorted it. Crucially, population receptive fields of early visual area voxels are on the order of several degrees, meaning the subjects would have had to have an eccentric fixation of several degrees to affect the cortical maps. Our subjects were anisometropic amblyopes and do not have monocular eccentric fixation of this magnitude.

Funding

This work was supported by the National Natural Science Foundation of China Grants NSFC 81500754 to Jiawei Zhou, NSFC 81261120562 to Yifeng Zhou and NSFC 81300796 to Lixia Feng; the Wenzhou Medical University grant QTJ16005 to Jiawei Zhou; Canadian Institutes of Health Research Grant CIHR CCI-125686 to Robert F. Hess; Startup funds from the RI-MUHC and an NSERC Discovery Award (RGPIN 419235-2013) to Reza Farivar. The funding organizations had no role in study design, data collection and analysis, decision to publish, or preparation of the manuscript. A subset of this data was used as part of another study by Yufeng Huang, Lixia Feng, Yifeng Zhou.

References

Aaen-Stockdale, C., Ledgeway, T., Hess, R.F., 2007. Second-order optic flow processing. Vis. Res. I47, 1798–1808.

Barnes, G.R., Hess, R.F., Dumoulin, S.O., Achtman, R.L., Pike, G.B., 2001. The cortical deficit in humans with strabismic amblyopia. J. Physiol. (Lond) 533, 281–297.

Bedell, H.D., Flom, M.C., 1981. Monocular spatial distortion in strabismic amblyopia. Invest. Ophthalmol. Vis. Sci. 20, 263–268.

Bedell, H.E., Flom, M.C., 1983. Normal and abnormal space perception. Am. J. Optom. Physiol. Opt. 60, 426–435.

Bedell, H.E., Flom, M.C., Barbeito, R., 1985. Spatial aberrations and acuity in strabismus and amblyopia. Invest. Ophthalmol. Vis. Sci. 26, 909–916.

Brainard, D.H., 1997. The psychophysics toolbox. Spat. Vis. 10, 433–436.

Chino, Y.M., Shansky, M.S., Jankowski, W.L., Banser, F.A., 1983. Effects of rearing kittens with convergent strabismus on development of receptive-field properties in striate cortex neurons. J. Neurophysiol. 50, 265–286.

Chung, S.T., Kumar, G., Li, R.W., Levi, D.M., 2015. Characteristics of fixational eye movements in amblyopia: limitations on fixation stability and acuity? Vis. Res. 114, 87–99.

Ciuffreda, K.J., Kenyon, R.V., Stark, L., 1979. Fixational eye movements in amblyopia and strabismus. J. Am. Optom. Assoc. 50, 1251–1258.

Ciuffreda, K.J., Levi, D.M., Selenow, A., 1991. Amblyopia: Basic and Clinical Aspects. Butterworth-Heinemann, Stoneham.

Clavagnier, S., Dumoulin, S.O., Hess, R.F., 2015. Is the cortical deficit in amblyopia due to reduced cortical magnification, loss of neural resolution or neural disorganization? J. Neurosci. 35, 14740–14755.

Cox, R.W., 1996. AFNI: software for analysis and visualization of functional magnetic resonance neuroimages. Comput. Biomed. Res. 29, 162–173.

Crewther, D.P., Crewther, S.G., 1990. Neural site of strabismic amblyopia in cats: spatial frequency deficit in primary cortical neurons. Exp. Brain Res. 79, 615–622.

Dale, A.M., Fischl, B., Sereno, M.I., 1999. Cortical surface-based analysis. I. Segmentation and surface reconstruction. Neuroimage 9, 179–194.

Eggers, H.M., Blakemore, C., 1978. Physiological basis of anisometropic amblyopia. Sci. (N Y) 201, 264–267.

Esterman, M., Yantis, S., 2010. Perceptual expectation evokes category-selective cortical activity. Cereb. Cortex 20, 1245–1253.

Fischl, B., Sereno, M.I., Dale, A.M., 1999. Cortical surface-based analysis. II: inflation, flattening, and a surface-based coordinate system. Neuroimage 9, 195–207.

Gingras, G., Mitchell, D.E., Hess, R.F., 2005a. Haphazard neural connections underlie the visual deficits of cats with strabismic or deprivation amblyopia. Eur. J. Neurosci. 22, 119–124.

Gingras, G., Mitchell, D.E., Hess, R.F., 2005b. The spatial localization deficit in visually deprived kittens. Vis. Res. 45, 975–989.

Gstalder, R.J., Green, D.G., 1971. Laser interferometric acuity in amblyopia. J. Pediatr. Ophthalmol. 8, 251–256.

Hess, R.F., 1982. Developmental sensory impairment: amblyopia or tarachopia? Hum. Neurobiol. 1, 17–29.

Hess, R.F., Campbell, F.W., Greenhalgh, T., 1978. On the nature of the neural abnormality in human amblyopia; neural aberrations and neural sensitivity loss. Pflug. Arch. Eur. J. Physiol. 377, 201–207.

Hess, R.F., Field, D.J., 1994. Is the spatial deficit in strabismic amblyopia due to loss of cells or an uncalibrated disarray of cells? Vis. Res. 34, 3397–3406.

Hess, R.F., Holliday, I.E., 1992. The spatial localization deficit in amblyopia. Vis. Res. 32, 1319–1339.

Hess, R.F., Howell, E.R., 1977. The threshold contrast sensitivity function in strabismic amblyopia: evidence for a two type classification. Vis. Res. 17, 1049–1055.

Hess, R.F., Li, X., Lu, G., Thompson, B., Hansen, B.C., 2010a. The contrast dependence of the cortical fMRI deficit in amblyopia; a selective loss at higher contrasts. Hum. Brain Mapp. 31, 1233–1248.

Hess, R.F., Thompson, B., Baker, D.H., 2014. Binocular vision in amblyopia: structure, suppression and plasticity. Ophthalmic Physiol. Opt. 34, 146–162.

Hess, R.F., Thompson, B., Gole, G.A., Mullen, K.T., 2010b. The amblyopic deficit and its relationship to geniculo-cortical processing streams. J. Neurophysiol. 104, 475–483.

Huk, A.C., Heeger, D.J., 2000. Task-related modulation of visual cortex. J. Neurophysiol. 83, 3525–3536.

Hussain, Z., Svensson, C.M., Besle, J., Webb, B.S., Barrett, B.T., McGraw, P.V., 2015. Estimation of cortical magnification from positional error in normally sighted and amblyopic subjects. J. Vis. 15 (25), 21–16.

Kiorpes, L., Boothe, R.G., Hendrickson, A.E., Movshon, J.A., Eggers, H.M., Gizzi, M.S., 1987. Effects of early unilateral blur on the macaque's visual system. I. Behavioral observations. J. Neurosci. 7, 1318–1326.

Kiorpes, L., Kiper, D.C., O'Keefe, L.P., Cavanaugh, J.R., Movshon, J.A., 1998. Neuronal correlates of amblyopia in the visual cortex of macaque monkeys with experimental strabismus and anisometropia. J. Neurosci. 18, 6411–6424.

Kiorpes, L., McKee, S.P., 1999. Neural mechanisms underlying amblyopia. Curr. Opin. Neurobiol. 9, 480–486.

Lagreze, W.D., Sireteanu, R., 1991. Two-dimensional spatial distortions in human strabismic amblyopia. Vis. Res. 31, 1271–1288.

Lerner, Y., Hendler, T., Malach, R., Harel, M., Leiba, H., Stolovitch, C., Pianka, P., 2006. Selective fovea-related deprived activation in retinotopic and high-order visual cortex of human amblyopes. Neuroimage 33, 169–179.

Lerner, Y., Pianka, P., Azmon, B., Leiba, H., Stolovitch, C., Loewenstein, A., Harel, M., Hendler, T., Malach, R., 2003. Area-specific amblyopic effects in human occipitotemporal object representations. Neuron 40, 1023–1029.

Levi, D.M., Klein, S., 1982. Hyperacuity and amblyopia. Nature 298, 268–270.

Levi, D.M., Klein, S.A., 1983. Spatial localization in normal and amblyopic vision. Vis. Res. 23, 1005–1017.

Levi, D.M., Klein, S.A., Aitsebaomo, A.P., 1985. Vernier acuity, crowding and cortical magnification. Vis. Res. 25, 963–977.

Levi, D.M., Klein, S.A., Yap, Y.L., 1987. Positional uncertainty in peripheral and amblyopic vision. Vis. Res. 27, 581–597.

Levi, D.M., Li, R.W., 2009. Perceptual learning as a potential treatment for amblyopia: a mini-review. Vis. Res. 49, 2535–2549.

Levi, M., Harwerth, R.S., 1977. Spatio-temporal interactions in anisometropic and strabismic amblyopia. Invest. Ophthalmol. Vis. Sci. 16, 90–95.

Li, X., Dumoulin, S.O., Mansouri, B., Hess, R.F., 2007a. Cortical deficits in human amblyopia: their regional distribution and their relationship to the contrast detection deficit. Invest. Ophthalmol. Vis. Sci. 48, 1575–1591.

Li, X., Dumoulin, S.O., Mansouri, B., Hess, R.F., 2007b. The fidelity of the cortical retinotopic map in human amblyopia. Eur. J. Neurosci. 25, 1265–1277.

Mansouri, B., Allen, H.A., Hess, R.F., 2005. detection, discrimination and integration of second-order orientation information in strabismic and anisometropic amblyopia. Vis. Res. 45, 2449–2460.

Mansouri, B., Hansen, B.C., Hess, R.F., 2009. Disrupted retinotopic maps in amblyopia. Invest. Ophthalmol. Vis. Sci. 50, 3218–3225.

Movshon, J.A., Eggers, H.M., Gizzi, M.S., Hendrickson, A.E., Kiorpes, L., Boothe, R.G., 1987. Effects of early unilateral blur on the macaque's visual system. III. Physiological observations. J. Neurosci. 7, 1340–1351.

Muckli, L., Kiess, S., Tonhausen, N., Singer, W., Goegel, R., Sireteanu, R., 2006. Cerebral correlates of impaired grating perception in individual psychophysically assessed human amblyopes. Vis. Res. 46, 506–526.

Niechwiej-Szwedo, E., Goltz, H.C., Chandrakumar, M., Hirji, Z.A., Wong, A.M., 2010. Effects of anisometropic amblyopia on visuomotor behavior, I: saccadic eye movements. Invest. Ophthalmol. Vis. Sci. 51, 6348–6354.

Pelli, D.G., 1997. The VideoToolbox software for visual psychophysics: transforming numbers into movies. Spat. Vis. 10, 437–442.

Reuter, M., Schmansky, N.J., Rosas, H.D., Fischl, B., 2012. Within-subject template estimation for unbiased longitudinal image analysis. Neuroimage 61, 1402–1418.

Saad, Z.S., Reynolds, R.C., 2012. Suma. Neuroimage 62, 768–773.

Sharma, V., Levi, D.M., Klein, S.A., 2000. Undercounting features and missing features: evidence for a high-level deficit in strabismic amblyopia. Nat. Neurosci. 3, 496–501.

Simmers, A.J., Ledgeway, T., Hess, R.F., McGraw, P.V., 2003. Deficits to global motion processing in human amblyopia. Vis. Res. 43, 729–738.

Sireteanu, R., Lagreze, W.D., Constantinescu, D.H., 1993. Distortions in two-dimensional visual space perception in strabismic observers. Vis. Res. 33, 677–690.

Sireteanu, R., Tonhausen, N., Mickli, L., Zanella, F.F., Singer, W., 1998. Cortical site of the amblyopic deficit in strabismic and anisometropic subjects investigated with fMRI. Invest. Ophthalmol. Vis. Sci. 39, s909.

Smith, A.T., Singh, K.D., Williams, A.L., Greenlee, M.W., 2001. Estimating receptive field size from fMRI data in human striate and extrastriate visual cortex. Cereb. Cortex 11, 1182–1190.

Tao, X., Zhang, B., Shen, G., Wensveen, J.M., Smith, R.E.L., Nishimoto, S., Ohzawa, I., Chino, Y., 2014. Early monocular defocus disrupts the normal development of receptive-field structure in V2 neurons of macaque monkeys. J. Neurosci. 34, 13840–13854.

Vanni, S., Henriksson, L., James, A., 2005. Multifocal fMRI mapping of visual cortical areas. Neuroimage 27, 95–105.

Warnking, J., Dojat, M., Guerin-Dugue, A., Delon-Martin, C., Olympieff, S., Richard, N., Chehikian, A., Segebarth, C., 2002. FMRI retinotopic mapping - step by step. Neuroimage 17, 1665–1683.